European Journal of Mechanics / A Solids 97 (2023) 104773

Contents lists available at ScienceDirect

European Journal of Mechanics / A Solids

journal homepage: www.elsevier.com/locate/ejmsol

Coupled thermal stability analysis of piezomagnetic nano-sensors and nano-actuators considering the flexomagnetic effect

Hamed Momeni-Khabisi [a], Masoud Tahani [a,b,*,1]

[a] Department of Mechanical Engineering, Ferdowsi University of Mashhad, Mashhad, Iran
[b] Institute of Fundamental Technological Research, Polish Academy of Sciences, Pawińskiego 5B, 02-106 Warsaw, Poland

ARTICLE INFO

Keywords:
Thermal buckling and post-buckling
Closed-form solution
Piezo-flexomagnetic plate strip
Size-dependent theories
Mid-plane initial rise

ABSTRACT

The current investigation deals with an analytical formulation and solution procedure for the thermal stability characteristics of piezomagnetic nano-sensors and nano-actuators considering the flexomagnetic effects and geometrical imperfection. Piezo-flexomagnetic nano-plate strips with the mid-plane initial rise are subjected to external uniform, linear, and nonlinear temperature rise loading across the thickness. The nonlinear size-dependent governing equations are derived within the framework of the first-order shear deformation plate theory, nonlocal strain gradient theory and considering the nonlinear von- Kármán strains. The proposed closed-form solutions and the obtained results are validated with the available data in the literature. The calculated buckling and post-buckling temperatures of piezo-flexomagnetic nano-plate strips are shown to be dependent on several factors including the scaling parameters, plate slenderness ratio, mid-plane initial rise, different temperature distributions, and scalar magnetic potential. The presented closed-form solutions and numerical results can serve as benchmarks for future analyses of piezo-flexomagnetic nano-sensors and nano-actuators.

1. Introduction

Smart materials have various applications in material science, mechanical industries, aerospace, military, nanotechnology, and biotechnology. Piezoelectric, piezomagnetic, flexoelectric, and flexomagnetic materials are the new types of smart materials that respond to external stimuli. These materials are ideal and applicable materials for smart magneto-electro-mechanical devices with a wide range of applications such as energy harvesting and fluid delivery systems. For example, Angelou et al. (2021) proposed a lead-free piezoelectric actuator as an insulin delivery micro-pump and Hu et al. (2022) to extend the operational life of cardiac pacemaker proposed a piezoelectric energy harvester design that can provide a power of 1 μW. They used a commercial finite element software to simulate and characterize these systems. By applying the uniform mechanical strain, the piezoelectric/piezomagnetic material changes the mechanical energy into an electric/magnetic field and vice-versa (Bahl et al., 2020; Karimiasl et al., 2019; Maurya et al., 2020; Moradi and Behdinan, 2020, 2021).

The coupling between the strain gradient and the induced electric field is known as the flexoelectric (FE) effect. Similarly, the flexomagnetic (FM) effect is defined as the coupling between the non-uniform mechanical strain and the induced magnetic field. The flexomagnetic effect can be divided into two categories: the direct flexomagnetic (DFM) effect and the converse flexomagnetic (CFM) effect. Inducing the magnetic field due to the strain gradient is defined as the DFM effect, while the CFM effect is the property of flexomagnetic materials to develop the mechanical strain in presence of the magnetic field gradient (Eliseev et al., 2009, 2019; Basutkar et al., 2019; Zhang et al., 2019).

One of the new research topics in the field of micro/nano-electromechanical systems (MEMs/NEMs) is the energy supply required by electronic devices such as portable components, medical implants, and wireless sensors. The use of wasted energies and its conversion into the required energy of these devices has received a lot of attention (Moradi-Dastjerdi and Behdinan, 2021). FM effect is not restricted to the crystalline symmetry, therefore this phenomenon expands the choice of materials that can be used for nano-sensors and nano-electromechanical actuators (Malikan et al., 2020).

Nano-scale sensors and actuators are the main part of advances in nanotechnology that play a crucial role in many industrial and medical devices. A lot of research is underway on the design and development of more efficient nano-sensors and nano-actuators with different accuracy (Wang et al., 2022; Moradi-Dastjerdi et al., 2019; Meschino et al., 2021; Mir and Tahani, 2020). The role of the strain gradient is more crucial

* Corresponding author at: Department of Mechanical Engineering, Ferdowsi University of Mashhad, Mashhad, Iran.
E-mail address: mtahani@um.ac.ir (M. Tahani).
[1] Professor.

https://doi.org/10.1016/j.euromechsol.2022.104773
Received 5 July 2022; Received in revised form 4 August 2022; Accepted 11 August 2022
Available online 17 August 2022

Nomenclature

$(N_{xx}, M_{xx}, Q_x, N_{xxz})$	Stress resultants
(u_0, w_0)	Displacements of a point on the mid-plane (z=0)
α	Coefficient of thermal expansion
β	Coefficient of hygroscopic (or moisture) expansion
ΔC	Percent moisture change
ΔT	Temperature change
η_{ijk}	Strain gradient components
l	Strain gradient parameter
$\mathbf{H}$	Magnetic field vector
$\mu = (e_0 a)^2$	Nonlocal parameter
ν	Poisson's ratio
ϕ	Rotation of a transverse normal about the y-axis
ψ	Scalar magnetic potential
σ_{ij}	Stress components
τ_{xxz}	Higher-order stress
ε_{ij}	Strain components
a_{33}	Components of magnetic permeability
A_{ij}	Extensional stiffness coefficients
B_z	Transverse components of magnetic induction vector
C_{55}	Shear modulus
D_{11}	Bending stiffness coefficient
d_{31}	Coefficient of piezomagnetic
E	Elasticity modulus
f_{14}	Coefficient of flexomagnetic
g_{113113}	Component of the strain gradient elasticity tensor
h	Thickness of the plate strip
K_s	Shear correction factor
$L = a$	Length of nano-plate strip along the x-axis
n	Power index of temperature variation function
N_{xx}^C, M_{xx}^C	Hygroscopic stress resultants
N_{xx}^T, M_{xx}^T	Thermal stress resultants
Q_{ij}	Coefficients of plane stress reduced stiffness
u	Axial component of the displacement field
w	Transverse component of the displacement field
w^*	Mid-plane initial rise

at the nanometer scale and especially in nano-structures with the flexomagnetic effect (Nicolenco et al., 2021). The flexomagnetic effect is closely related to strain gradient and magnetic field. Some research works (Momeni-Khabisi and Tahani, 2022; Sidhardh and Ray, 2018; Zhang et al., 2019) have confirmed that the flexomagnetic effect can be more important at the nano-scale than at the macro-scale. In fact, compared to the piezomagnetic effect, the macro-scale flexomagnetic effect is usually relatively weak. Nevertheless, the flexomagnetic effect gradually becomes remarkable as the scale decreases. On the other hand, a nano-structure may be consciously or unconsciously exposed to an external magnetic field, and this field will undoubtedly affect its performance. Therefore, when examining magneto-mechanical coupling at the nano-scale, it is necessary to consider the flexomagnetic effect in order to avoid errors in the applications of nano-structures and perform a more appropriate design, and its performance on the mechanical behavior of nano-structures should be studied in different conditions (Malikan and Eremeyev, 2022a; Zhang et al., 2022a,b).

Also, the effect of thermal expansion is more important in nano-scale materials and the magnetization of the ferromagnetic material will increase upon heating. Thermal buckling is the reason for the failure of many structures that are exposed to high-temperature differences (Cai et al., 2020; Malikan et al., 2021).

Thermal buckling and post-buckling are of interest to many researchers. Ebnali Samani and Tadi Beni (2018) presented the thermal and mechanical pre-buckling of flexoelectric nanobeam based on the Timoshenko beam model. They investigated the effect of some parameters such as the dimensionless length to thickness, length scale parameter, and flexoelectric coefficient on the critical buckling load and critical temperature. Barati and Zenkour (2019) investigated thermal post-buckling analysis of piezoelectric nanobeam considering the inverse flexoelectric and surface effects. The Euler–Bernoulli beam theory with simply supported and clamped boundary conditions was used. They assumed the mid-span initial rise as geometrical imperfection. Tocci Monaco et al. (2021) analyzed hygrothermal buckling and vibration of simply supported cross- and angle-ply laminated composite nano-plates. They used the second-order strain gradient theory and Hamilton's principle based on the classical plate theory (CPT). Behdinan and Moradi-Dastjerdi (2022) studied the thermal buckling of active sandwich plate made of porous polymeric core and lead-free piezoelectric face sheets. They obtained the governing equations by adopting a higher-order theory of plates and they solved these equations by employing a mesh-free method.

There is little research on the FM effect and this field is still in its infancy (e.g., Shi et al., 2021; Sidhardh and Ray, 2018; Zhang et al., 2019, and references therein). Among them, Malikan et al. (2021) performed research on the size-dependent thermal stability of microbeams considering the piezomagneticity and converse flexomagneticity effects with three types of temperature distributions across the thickness. To derive the governing differential equations, they used the principle of virtual displacement, linear strains, and the second strain gradient theory of elasticity. They presented closed-form relations for the thermal buckling load in case of fully clamped and simply supported boundary conditions. Malikan et al. (2021b) studied the linear thermal buckling of functionally graded piezomagnetic Timoshenko micro- and nanobeams considering the converse flexomagnetic properties. They solved the size-dependent governing equations of equilibrium by the Galerkin weighted residual method for clamped boundary conditions. In their research, the effects of strain gradient and scaling parameters were formulated by the nonlocal strain gradient (NSG) theory. Recently, Momeni-Khabisi and Tahani (2022) investigated linear and nonlinear buckling behaviors of piezo-flexomagnetic nano-plate strips considering geometrical imperfection. Using the NSG theory and a variational method, they derived the size-dependent governing equations and related boundary conditions. A closed-form solution was presented and the effect of several parameters were studied. More recently, Malikan and Eremeyev (2022b) proposed a more general relation for free energy of a piezo-flexomagnetic structure. They used the differential and integral forms of nonlocal elasticity theory to study the buckling behavior of beams using a higher-order shear deformation theory.

Thermal buckling and post-buckling analysis of piezo-flexomagnetic (PFM) nano-plate strips have not been done yet. Furthermore, in this research, the first-order shear deformation plate theory (FSDPT), both direct and converse flexomagnetic effects, hygrothermal environment, and geometrical imperfection are considered simultaneously. To derive the nonlinear size-dependent governing equations, the von- Kármán strains, NSG theory, and principle of minimum total potential energy are used. A parametric study is presented, and the thermal buckling and post-buckling behavior of nano-sensors and nano-actuators are characterized by investigating several parameters such as the scaling parameters (nonlocal and length scale parameters), plate slenderness ratio (the ratio of the length along the x-axis to the thickness), mid-plane initial rise, different temperature distributions, and magnetic potential. To the extent of the authors' knowledge, there is no research considering such conditions simultaneously.

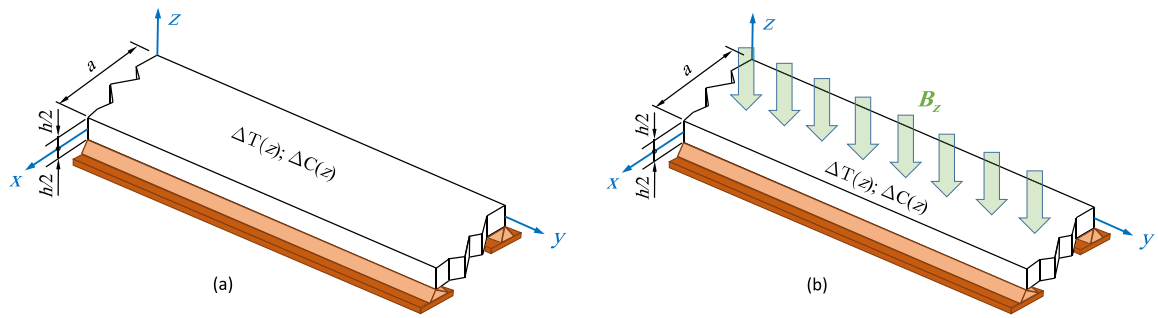

Fig. 1. Schematic of a piezo-flexomagnetic nano-plate strip under hygrothermal load and simply supported end conditions. (a) The DFM effect as a sensor, (b) the CFM effect as an actuator.

Table 1
Magneto-mechanical coefficients of material properties (Malikan et al., 2021).

$CoFe_2O_4$
$E = 286$ GPa, $\nu = 0.32$
$d_{31} = 580.3$ N/(A m), $a_{33} = 157 \times 10^{-6}$ N/A^2
$f_{14} = 10^{-9}$ N/A, $h = 1$ nm
$\alpha = 11.8 \times 10^{-6}$ 1/K

2. Modeling of the problem

Due to the magneto-elastic effect, when the ferromagnetic material is subjected to mechanical stress, its internal deformation leads to changes in magnetic permeability. By detecting these changes, mechanical stress can be measured. It is very important to measure the forces acting on the components in MEMs/NEMs during assembly because if the contact force is not reliably detected and controlled, the small-scale components are easily damaged during manipulation and assembly (Rasilo et al., 2019; Wei and Xu, 2015). Nano-structures may be inevitably or accidentally affected by the temperature that it may cause significant stresses and deformations. One of the important problems that arise due to the increase in temperature is thermal buckling. Without considering the effect of temperature, the design of the structure will not be safe and complete (Malikan et al., 2021). In this paper, we seek a relationship to obtain the critical temperature as well as the thermal post-buckling behavior of the nano-plate strip.

2.1. Basic formulation

In this section, magneto-hygro-thermal responses of PFM nano-plate strips are investigated utilizing the NSG theory. This model is illustrated in Fig. 1 and the properties of materials are given in Table 1. Consider a rectangular plate strip in the x-y plane that the width b along the y-axis is very long compared to the length a along the x-axis. It is necessary to mention that, as is stated in Reddy (2006), the plate strip is a case of plates that can be treated as a one-dimensional structure, it is assumed that one planar dimension of the plate is long and the other planar dimension is relatively smaller, but it is considerably large compared to the thickness. The displacements of such plate strips are only a function of the smaller planar dimension. In case of beams, the width b is very small compared to the length a.

The plate strip is simply-supported along the edges $x = 0, a$ and it is in a hygrothermal environment. The temperature and moisture distribution through the thickness are defined as Eq. (31). It should be noted that three uniform, linear and quadratic distributions are considered for temperature in this paper. For the completeness of the derived equations, the effect of moisture has also been applied but due to the lack of data on the coefficient of moisture expansion of cobalt ferrite in the literature, the effect of moisture in the numerical results has not been considered in this paper. The mechanical and magnetic boundary conditions are presented in Eq. (12).

Based on the first-order shear deformation plate theory, the components of the displacement field are defined as:

$$\begin{aligned} u(x,z) &= u_0(x) + z\phi(x) \\ w(x,z) &= w_0(x) \end{aligned} \tag{1}$$

In the present study we also wish to investigate the effect of geometric non-linearity on the response quantities. Therefore, the von Kármán-type of geometric non-linearity is taken into consideration in the strain–displacement relations. Substituting Eqs. (1) in the appropriate strain–displacement relations results in:

$$\begin{aligned} \varepsilon_{xx} &= \varepsilon^0_{xx} + z\varepsilon^1_{xx} \\ \gamma_{xz} &= \gamma^0_{xz} \\ \varepsilon_{yy} &= \varepsilon_{zz} = \gamma_{xy} = \gamma_{yz} = 0 \\ \eta_{xxz} &= \frac{d\phi}{dx} \\ \eta_{yyz} &= \eta_{xyz} = 0 \end{aligned} \tag{2}$$

where

$$\begin{aligned} \varepsilon^0_{xx} &= \frac{du_0}{dx} + \frac{1}{2}\left(\frac{dw_0}{dx}\right)^2 \\ \gamma^0_{xz} &= \phi + \frac{dw_0}{dx} \\ \varepsilon^1_{xx} &= \frac{d\phi}{dx} \end{aligned} \tag{3}$$

The magnetic field vector $\mathbf{H}$ is related to the scalar magnetic potential as below:

$$\mathbf{H} = -\nabla\psi \tag{4}$$

Considering the effects of the temperature and moisture, the constitutive equations can be written as Reddy (2006), Shi et al. (2021), Sidhardh and Ray (2018) and Wang and Li (2021):

$$\begin{aligned} \sigma_{xx} &= Q_{11}\left(\varepsilon_{xx} - \alpha\Delta T - \beta\Delta C\right) + Q_{12}\left(\varepsilon_{yy} - \alpha\Delta T - \beta\Delta C\right) - d_{31}H_z \\ \sigma_{xz} &= C_{55}\gamma_{xz} \\ \tau_{xxz} &= g_{113113}\eta_{xxz} - f_{14}H_z \\ B_z &= a_{33}H_z + d_{31}\varepsilon_{xx} + f_{14}\eta_{xxz} \end{aligned} \tag{5}$$

where Q_{ij} are the plane stress reduced stiffness coefficients, α and β are the coefficients of thermal and hygroscopic expansion, respectively. The first variation of the free energy can be written as follows:

$$\delta U = \int_A \int_{-h/2}^{h/2} \left(\sigma_{xx}\delta\varepsilon_{xx} + \sigma_{xz}\delta\gamma_{xz} + \tau_{xxz}\delta\eta_{xxz} - B_z\delta H_z\right) dz dA \tag{6}$$

Combining Eqs. (2), (3), (4), and (6) and using the divergence theorem, we obtain:

$$\delta U = \int_A \left[-\frac{dN_{xx}}{dx}\delta u_0 - \frac{d}{dx}\left(N_{xx}\frac{dw_0}{dx}\right)\delta w_0 - \frac{dM_{xx}}{dx}\delta\phi + Q_x\delta\phi - \frac{dQ_x}{dx}\delta w_0 - \frac{dN_{xxz}}{dx}\delta\phi\right] dA$$

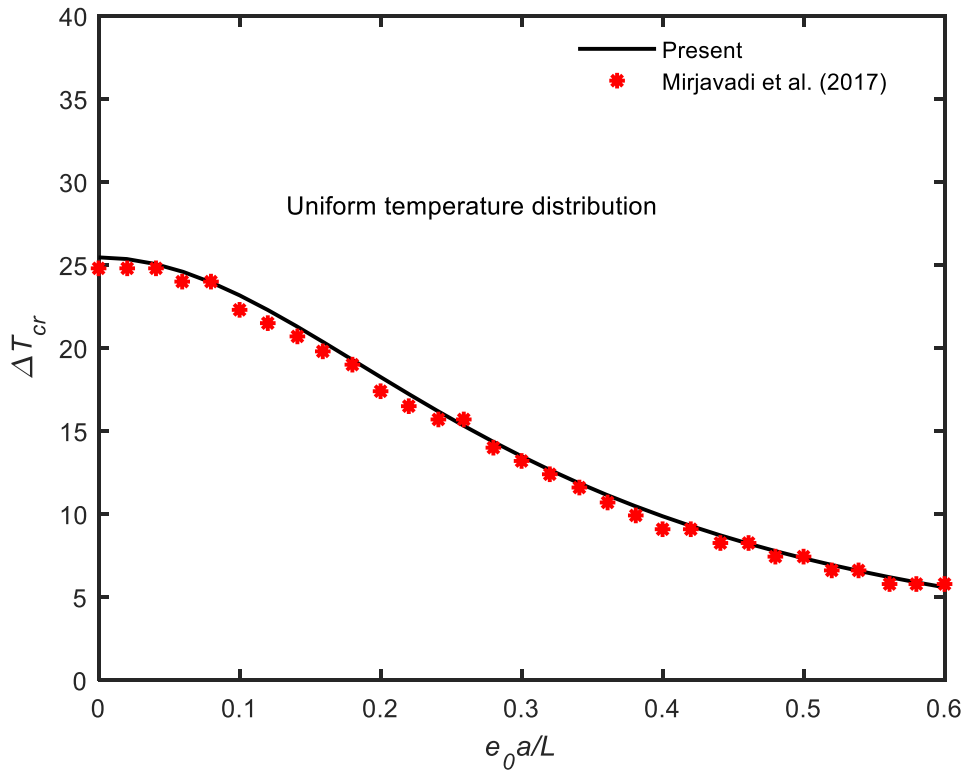

Fig. 2. The variations of critical buckling temperature of simply supported AFG nanobeam vs. non-dimensional nonlocal parameter.

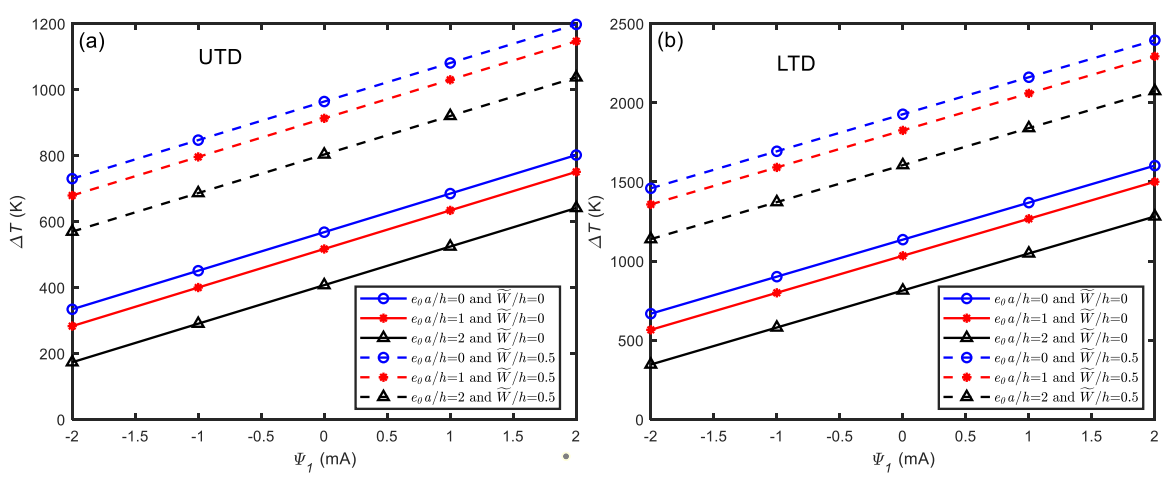

Fig. 3. Buckling and post-buckling temperatures vs. scalar magnetic potential at different nonlocal parameters for the CFM case. (a) Uniform temperature distribution (UTD), (b) linear temperature distribution (LTD).

$$-\int_A\int_{-h/2}^{h/2}\frac{\partial B_z}{\partial z}\delta\psi \mathrm{d}z\mathrm{d}A+\left[\int_0^b\left(N_{xx}\delta u_0+N_{xx}\frac{\mathrm{d}w_0}{\mathrm{d}x}\delta w_0+M_{xx}\delta\phi+Q_x\delta w_0+N_{xxz}\delta\phi\right)\mathrm{d}y\right]_{x=0}^{x=a}+\left[\int_A B_z\delta\psi\mathrm{d}A\right]_{z=-h/2}^{z=h/2} \tag{7}$$

By applying the principle of minimum total potential energy, the equilibrium equations are obtained as:

$$\delta u_0: \quad \frac{\mathrm{d}N_{xx}}{\mathrm{d}x}=0 \tag{8}$$

$$\delta w_0: \quad \frac{\mathrm{d}}{\mathrm{d}x}\left(N_{xx}\frac{\mathrm{d}w_0}{\mathrm{d}x}\right)+\frac{\mathrm{d}Q_x}{\mathrm{d}x}=0 \tag{9}$$

$$\delta\phi: \quad \frac{\mathrm{d}M_{xx}}{\mathrm{d}x}+\frac{\mathrm{d}N_{xxz}}{\mathrm{d}x}-Q_x=0 \tag{10}$$

$$\delta\psi: \quad \frac{\partial B_z}{\partial z}=0 \tag{11}$$

The boundary conditions involve the specification of

$$\begin{aligned}
&\delta u_0=0 \quad \text{or} \quad N_{xx}=0 && at\ \ x=0,a\\
&\delta w_0=0 \quad \text{or} \quad N_{xx}\frac{\mathrm{d}w_0}{\mathrm{d}x}+Q_x=0 && at\ \ x=0,a\\
&\delta\phi=0 \quad \text{or} \quad M_{xx}+N_{xxz}=0 && at\ \ x=0,a\\
&\psi=\Psi_1 \quad \text{or} \quad B_z=0 && at\ \ z=\pm\frac{h}{2}
\end{aligned} \tag{12}$$

where the stress resultants are defined as:

$$\left(N_{xx}, M_{xx}\right) = \int_{-h/2}^{h/2} \sigma_{xx}\left(1, z\right) \mathrm{d}z$$
$$Q_x = K_s \int_{-h/2}^{h/2} \sigma_{xz} \mathrm{d}z, \quad N_{xxz} = \int_{-h/2}^{h/2} \tau_{xxz} \mathrm{d}z \tag{13}$$

2.2. Flexomagnetic sensors

Fig. 1(a) shows the DFM effect as a sensor, in which mechanical stress (here thermal stress) leads to the change of magnetic properties and as a result, creation of a magnetic field. Using Eqs. (11) and (12), we conclude that:

$$B_z = 0 \text{ throughout the body} \tag{14}$$

Using Eqs. (2)–(5) and (14) one can get:

$$\psi\left(x, z\right) = \frac{d_{31}}{a_{33}}\left[\frac{\mathrm{d}u_0}{\mathrm{d}x} + \frac{1}{2}\left(\frac{\mathrm{d}w_0}{\mathrm{d}x}\right)^2 + \frac{f_{14}}{d_{31}}\frac{\mathrm{d}\phi}{\mathrm{d}x}\right] z + \frac{d_{31}}{a_{33}}\frac{\mathrm{d}\phi}{\mathrm{d}x}\frac{z^2}{2} + C_0 \tag{15}$$

$$H_z = -\frac{\partial \psi}{\partial z} = -\frac{d_{31}}{a_{33}}\left[\frac{\mathrm{d}u_0}{\mathrm{d}x} + \frac{1}{2}\left(\frac{\mathrm{d}w_0}{\mathrm{d}x}\right)^2 + z\frac{\mathrm{d}\phi}{\mathrm{d}x}\right] - \frac{f_{14}}{a_{33}}\frac{\mathrm{d}\phi}{\mathrm{d}x} \tag{16}$$

Therefore, the higher-order and classical stresses are determined as follows:

$$\sigma_{xx} = \left(Q_{11} + \frac{d_{31}^2}{a_{33}}\right)\left[\frac{\mathrm{d}u_0}{\mathrm{d}x} + \frac{1}{2}\left(\frac{\mathrm{d}w_0}{\mathrm{d}x}\right)^2\right] + \left(Q_{11} + \frac{d_{31}^2}{a_{33}}\right) z\frac{\mathrm{d}\phi}{\mathrm{d}x}$$
$$- \left(Q_{11} + Q_{12}\right)\left(\alpha\Delta T + \beta\Delta C\right) + \frac{f_{14}d_{31}}{a_{33}}\frac{\mathrm{d}\phi}{\mathrm{d}x} \tag{17}$$

$$\sigma_{xz} = C_{55}\left(\frac{\mathrm{d}w_0}{\mathrm{d}x} + \phi\right) \tag{18}$$

$$\tau_{xxz} = \left(g_{113113} + \frac{f_{14}^2}{a_{33}}\right)\frac{\mathrm{d}\phi}{\mathrm{d}x} + \frac{f_{14}d_{31}}{a_{33}}\left[\frac{\mathrm{d}u_0}{\mathrm{d}x} + \frac{1}{2}\left(\frac{\mathrm{d}w_0}{\mathrm{d}x}\right)^2 + z\frac{\mathrm{d}\phi}{\mathrm{d}x}\right] \tag{19}$$

Considering the mid-plane initial rise w^* and using Eqs. (8), (12), (13), and (17)–(19) the stress resultants can be obtained as:

$$N_{xx} = \hat{N}_{xx} = \frac{A_{11}a_{33} + hd_{31}^2}{a_{33}}\frac{1}{2a}\int_0^a \left[\left(\frac{\mathrm{d}w}{\mathrm{d}x}\right)^2 - \left(\frac{\mathrm{d}w^*}{\mathrm{d}x}\right)^2\right]\mathrm{d}x$$
$$- \frac{1}{a}\int_0^a \left(N_{xx}^T + N_{xx}^C\right)\mathrm{d}x \tag{20}$$

$$M_{xx} = \left(D_{11} + \frac{h^3}{12}\frac{d_{31}^2}{a_{33}}\right)\frac{\mathrm{d}\phi}{\mathrm{d}x} - \left(M_{xx}^T + M_{xx}^C\right) \tag{21}$$

$$N_{xxz} = \bar{g}\frac{\mathrm{d}\phi}{\mathrm{d}x} + \frac{hf_{14}d_{31}}{a_{33}}\frac{1}{2a}\int_0^a \left[\left(\frac{\mathrm{d}w}{\mathrm{d}x}\right)^2 - \left(\frac{\mathrm{d}w^*}{\mathrm{d}x}\right)^2\right]\mathrm{d}x$$
$$+ \frac{hf_{14}d_{31}}{A_{11}a_{33} + hd_{31}^2}\left[\left(N_{xx}^T + N_{xx}^C\right) - \frac{1}{a}\int_0^a \left(N_{xx}^T + N_{xx}^C\right)\mathrm{d}x\right] \tag{22}$$

$$Q_x = K_s A_{55}\left(\frac{\mathrm{d}w}{\mathrm{d}x} - \frac{\mathrm{d}w^*}{\mathrm{d}x} + \phi\right) \tag{23}$$

where

$$Q_{11} = \frac{E}{1-\nu^2}, \quad Q_{12} = \frac{E\nu}{1-\nu^2} \tag{24}$$

$$A_{11} = \int_{-h/2}^{h/2} Q_{11}\mathrm{d}z = Q_{11}h, \quad A_{55} = \int_{-h/2}^{h/2} C_{55}\mathrm{d}z = C_{55}h,$$
$$D_{11} = \int_{-h/2}^{h/2} Q_{11}z^2\mathrm{d}z = \frac{Q_{11}h^3}{12}, \quad g_{113113} = \frac{29Q_{11}(1-\nu)l^2}{30} \tag{25}$$

$$N_{xx}^T = \int_{-h/2}^{h/2} \left(Q_{11} + Q_{12}\right)\alpha\Delta T\mathrm{d}z, \quad M_{xx}^T = \int_{-h/2}^{h/2} \left(Q_{11} + Q_{12}\right)\alpha\Delta T z\mathrm{d}z,$$
$$N_{xx}^C = \int_{-h/2}^{h/2} \left(Q_{11} + Q_{12}\right)\beta\Delta C\mathrm{d}z, \quad M_{xx}^C = \int_{-h/2}^{h/2} \left(Q_{11} + Q_{12}\right)\beta\Delta C z\mathrm{d}z \tag{26}$$

$$\bar{g} = \hat{g}_{113113} + \frac{hf_{14}^2 A_{11}}{A_{11}a_{33} + hd_{31}^2}, \quad \hat{g}_{113113} = \int_{-h/2}^{h/2} g_{113113}\mathrm{d}z = g_{113113}h \tag{27}$$

Using the NSG theory and combining Eqs. (8)–(10), and (20), the governing differential equations of PFM nano-plate strips considering the size-dependency, direct FM effect, mid-plane initial rise, and shear deformation are obtained as:

$$K_s A_{55}\left(\frac{\mathrm{d}^2 w}{\mathrm{d}x^2} - \frac{\mathrm{d}^2 w^*}{\mathrm{d}x^2} + \frac{\mathrm{d}\phi}{\mathrm{d}x}\right) - l^2 K_s A_{55}\left(\frac{\mathrm{d}^4 w}{\mathrm{d}x^4} - \frac{\mathrm{d}^4 w^*}{\mathrm{d}x^4} + \frac{\mathrm{d}^3\phi}{\mathrm{d}x^3}\right)$$
$$+ \left(\frac{\mathrm{d}^2 w}{\mathrm{d}x^2} - \mu\frac{\mathrm{d}^4 w}{\mathrm{d}x^4}\right)$$
$$\times\left\{\frac{A_{11}a_{33} + hd_{31}^2}{a_{33}}\frac{1}{2a}\int_0^a \left[\left(\frac{\mathrm{d}w}{\mathrm{d}x}\right)^2 - \left(\frac{\mathrm{d}w^*}{\mathrm{d}x}\right)^2\right]\mathrm{d}x\right.$$
$$\left. - \frac{1}{a}\int_0^a \left(N_{xx}^T + N_{xx}^C\right)\mathrm{d}x\right\} = 0 \tag{28}$$

$$-\left(\frac{\mathrm{d}M_{xx}^T}{\mathrm{d}x} + \frac{\mathrm{d}M_{xx}^C}{\mathrm{d}x}\right) + \overline{\widetilde{D}}\frac{\mathrm{d}^2\phi}{\mathrm{d}x^2} - K_s A_{55}\left(\frac{\mathrm{d}w}{\mathrm{d}x} - \frac{\mathrm{d}w^*}{\mathrm{d}x} + \phi\right)$$
$$- l^2\left[-\frac{\mathrm{d}^3 M_{xx}^T}{\mathrm{d}x^3} - \frac{\mathrm{d}^3 M_{xx}^C}{\mathrm{d}x^3} + \overline{\widetilde{D}}\frac{\mathrm{d}^4\phi}{\mathrm{d}x^4} - K_s A_{55}\left(\frac{\mathrm{d}^3 w}{\mathrm{d}x^3} - \frac{\mathrm{d}^3 w^*}{\mathrm{d}x^3} + \frac{\mathrm{d}^2\phi}{\mathrm{d}x^2}\right)\right] = 0 \tag{29}$$

where

$$\overline{\widetilde{D}} = D_{11} + \frac{h^3}{12}\frac{d_{31}^2}{a_{33}} + \bar{g} \tag{30}$$

Assuming the temperature and moisture distributions through the thickness as below:

$$\Delta T\left(z\right) = \left(\frac{z + h/2}{h}\right)^n \left(T - T_0\right), \quad -h/2 \le z \le h/2, \ 0 \le n \le \infty$$
$$\Delta C\left(z\right) = \left(\frac{z + h/2}{h}\right)^n \left(C - C_0\right), \quad -h/2 \le z \le h/2, \ 0 \le n \le \infty \tag{31}$$

and substituting Eq. (31) into Eq. (26) one can write the hygrothermal resultants as follows:

$$N_{xx}^T = A_T\left(T - T_0\right), \quad M_{xx}^T = D_T\left(T - T_0\right)$$
$$N_{xx}^C = A_C\left(C - C_0\right), \quad M_{xx}^C = D_C\left(C - C_0\right) \tag{32}$$

where $T - T_0$ and $C - C_0$ are temperature and moisture rise from the reference temperature and moisture T_0 and C_0 at which there are no hygrothermal strains and

$$A_T = \frac{Q_{11}\alpha\left(1+\nu\right)h}{1+n}, \quad A_C = \frac{Q_{11}\beta\left(1+\nu\right)h}{1+n}$$
$$D_T = \frac{Q_{11}\alpha\left(1+\nu\right)h^2 n}{2\left(1+n\right)\left(2+n\right)}, \quad D_C = \frac{Q_{11}\beta\left(1+\nu\right)h^2 n}{2\left(1+n\right)\left(2+n\right)} \tag{33}$$

Therefore, Eqs. (28) and (29) are simplified to

$$K_s A_{55}\left[\frac{\mathrm{d}^2 w}{\mathrm{d}x^2} - \frac{\mathrm{d}^2 w^*}{\mathrm{d}x^2} + \frac{\mathrm{d}\phi}{\mathrm{d}x} - l^2\left(\frac{\mathrm{d}^4 w}{\mathrm{d}x^4} - \frac{\mathrm{d}^4 w^*}{\mathrm{d}x^4} + \frac{\mathrm{d}^3\phi}{\mathrm{d}x^3}\right)\right]$$
$$+ \left\{\frac{A_{11}a_{33} + hd_{31}^2}{a_{33}}\frac{1}{2a}\int_0^a \left[\left(\frac{\mathrm{d}w}{\mathrm{d}x}\right)^2 - \left(\frac{\mathrm{d}w^*}{\mathrm{d}x}\right)^2\right]\mathrm{d}x - N_{xx}^T - N_{xx}^C\right\}$$

$$\times\left(\frac{d^2w}{dx^2}-\mu\frac{d^4w}{dx^4}\right)=0 \tag{34}$$

$$\overline{\widetilde{D}}\left(\frac{d^2\phi}{dx^2}-l^2\frac{d^4\phi}{dx^4}\right)-K_sA_{55}\left[\frac{dw}{dx}-\frac{dw^*}{dx}+\phi-l^2\times\left(\frac{d^3w}{dx^3}-\frac{d^3w^*}{dx^3}+\frac{d^2\phi}{dx^2}\right)\right]=0 \tag{35}$$

2.3. Flexomagnetic actuators

Fig. 1(b) shows the CFM effect as an actuator, in which the effect of the external magnetic field causes mechanical strain. The transverse magnetic field is constant through the thickness (see Eq. (11)). In case of CFM effect, the boundary conditions are expressed as (see Eq. (12)):

$$\psi(x,z=h/2)=\Psi_1,\quad \psi(x,z=-h/2)=0 \tag{36}$$

Using Eqs. (2)–(5), (11), and (36) the scalar magnetic potential and the magnetic field vector through the thickness of nano-plate strips are obtained as:

$$\begin{aligned}\psi(x,z)&=\frac{d_{31}}{2a_{33}}\left(z^2-\frac{h^2}{4}\right)\frac{d\phi}{dx}+\frac{\Psi_1}{h}\left(z+\frac{h}{2}\right)\\ H_z&=-z\frac{d_{31}}{a_{33}}\frac{d\phi}{dx}-\frac{\Psi_1}{h}\end{aligned} \tag{37}$$

Considering the mid-plane initial rise, the stress resultants are determined as follows:

$$\begin{aligned}N_{xx}&=\hat{N}_{xx}=-\frac{1}{a}\int_0^a\left(N_{xx}^T+N_{xx}^C\right)dx\\&\quad+\frac{A_{11}}{2a}\int_0^a\left[\left(\frac{dw}{dx}\right)^2-\left(\frac{dw^*}{dx}\right)^2\right]dx+d_{31}\Psi_1\\ M_{xx}&=-\left(M_{xx}^T+M_{xx}^C\right)+\left(D_{11}+\frac{h^3}{12}\frac{d_{31}^2}{a_{33}}\right)\frac{d\phi}{dx}\\ Q_x&=K_sA_{55}\left(\frac{dw}{dx}-\frac{dw^*}{dx}+\phi\right)\\ N_{xxz}&=\hat{g}_{113113}\frac{d\phi}{dx}+f_{14}\Psi_1\end{aligned} \tag{38}$$

where $A_{11}, A_{55}, D_{11}, \hat{g}_{113113}, N_{xx}^T, N_{xx}^C, M_{xx}^T$, and M_{xx}^C are defined in Eqs. (25)–(27).

After some mathematical operations similar to Section 2.2, the governing equations in case of the CFM effect are obtained as:

$$\begin{aligned}&K_sA_{55}\left(\frac{d^2w}{dx^2}-\frac{d^2w^*}{dx^2}+\frac{d\phi}{dx}\right)-l^2K_sA_{55}\left(\frac{d^4w}{dx^4}-\frac{d^4w^*}{dx^4}+\frac{d^3\phi}{dx^3}\right)\\&+\left(\frac{d^2w}{dx^2}-\mu\frac{d^4w}{dx^4}\right)\\&\times\left\{\frac{A_{11}}{2a}\int_0^a\left[\left(\frac{dw}{dx}\right)^2-\left(\frac{dw^*}{dx}\right)^2\right]dx\right.\\&\left.-\frac{1}{a}\int_0^a\left(N_{xx}^T+N_{xx}^C\right)dx+d_{31}\Psi_1\right\}=0\end{aligned} \tag{39}$$

$$\begin{aligned}&-\left(\frac{dM_{xx}^T}{dx}+\frac{dM_{xx}^C}{dx}\right)+\widetilde{D}\frac{d^2\phi}{dx^2}-K_sA_{55}\left(\frac{dw}{dx}-\frac{dw^*}{dx}+\phi\right)\\&-l^2\left[-\frac{d^3M_{xx}^T}{dx^3}-\frac{d^3M_{xx}^C}{dx^3}+\widetilde{D}\frac{d^4\phi}{dx^4}\right.\\&\left.-K_sA_{55}\left(\frac{d^3w}{dx^3}-\frac{d^3w^*}{dx^3}+\frac{d^2\phi}{dx^2}\right)\right]=0\end{aligned} \tag{40}$$

where

$$\widetilde{D}=D_{11}+\frac{h^3}{12}\frac{d_{31}^2}{a_{33}}+\hat{g}_{113113} \tag{41}$$

Combining Eqs. (39) and (40) with Eq. (31) one can simplify these equations as follows:

$$\begin{aligned}&K_sA_{55}\left[\frac{d^2w}{dx^2}-\frac{d^2w^*}{dx^2}+\frac{d\phi}{dx}-l^2\left(\frac{d^4w}{dx^4}-\frac{d^4w^*}{dx^4}+\frac{d^3\phi}{dx^3}\right)\right]\\&+\left(\frac{d^2w}{dx^2}-\mu\frac{d^4w}{dx^4}\right)\\&\times\left\{\frac{A_{11}}{2a}\int_0^a\left[\left(\frac{dw}{dx}\right)^2-\left(\frac{dw^*}{dx}\right)^2\right]dx-N_{xx}^T-N_{xx}^C+d_{31}\Psi_1\right\}=0\end{aligned} \tag{42}$$

$$\begin{aligned}&\widetilde{D}\left(\frac{d^2\phi}{dx^2}-l^2\frac{d^4\phi}{dx^4}\right)-K_sA_{55}\left[\frac{dw}{dx}-\frac{dw^*}{dx}+\phi-l^2\times\left(\frac{d^3w}{dx^3}-\frac{d^3w^*}{dx^3}+\frac{d^2\phi}{dx^2}\right)\right]=0\end{aligned} \tag{43}$$

3. Solution procedure

The closed-form solution of the governing equations in case of direct and converse flexomagnetic effects is obtained by using the Navier method. To this aim, the following functions are considered:

$$\begin{aligned}&w(x)=\sum_{m=1}^{\infty}\widetilde{W}\sin\left(\frac{m\pi x}{a}\right),\ w^*(x)=W^*\sin\left(\frac{\pi x}{a}\right),\ \phi(x)\\&=\sum_{m=1}^{\infty}\tilde{\phi}\cos\left(\frac{m\pi x}{a}\right)\end{aligned} \tag{44}$$

It is worth mentioning that the mid-plane initial rise is considered as a half-sine wave. Upon substitution of Eq. (44) into Eqs. (35) and (43) one can obtain:

$$\tilde{\phi}=-\frac{K_sA_{55}\frac{m\pi}{a}\left(\widetilde{W}-W^*\right)}{\widehat{D}\left(\frac{m\pi}{a}\right)^2+K_sA_{55}} \tag{45}$$

By Combining Eqs. (45), (34), and (42) the thermal post-buckling formula is obtained as:

$$T=\frac{1}{A_T}\left[\frac{\widehat{D}\alpha_m{}^2\lambda_{lm}}{\Lambda\lambda_{\mu m}}\frac{\widetilde{W}-W^*}{\widetilde{W}}+\widehat{A}\alpha_m{}^2\left(\widetilde{W}^2-W^{*2}\right)+N^M-N_{xx}^C\right] \tag{46}$$

where $\Lambda=1+\widehat{D}\alpha_m{}^2/\left(K_sA_{55}\right)$, $\alpha_m=m\pi/a, \lambda_{lm}=1+l^2\alpha_m{}^2$, and $\lambda_{\mu m}=1+\mu\alpha_m{}^2$ and the numerical results are calculated for the first buckling mode (m=1).

In case of the DFM effect we have:

$$\widehat{D}=\overline{\widetilde{D}},\ \widehat{A}=\frac{A_{11}a_{33}+hd_{31}^2}{4a_{33}},\ N^M=0 \tag{47}$$

and the above parameters in case of the CFM effect are defined as:

$$\widehat{D}=\widetilde{D},\ \widehat{A}=\frac{A_{11}}{4},\ N^M=d_{31}\Psi_1 \tag{48}$$

Note that, for classical plate theory, $\Lambda=1$.

4. Validation

In this section, the accuracy of the proposed solution is validated by several methods.

In case of PFM thin microbeams without geometrical imperfection, moisture effects, and nonlocal parameter, the critical temperature of Eq. (46) can be reduced to that derived by Malikan et al. (2021) for the CFM case:

$$T=\frac{1}{A_T}\left(\widehat{D}\alpha_m{}^2\lambda_{lm}+N^M\right)=\frac{N^{Mag}L^4+DL^2\pi^2m^2+Dl^2\pi^4m^4}{\beta L^4} \tag{49}$$

Numerical results based on presented closed-form solution are tabulated in Table 2. It should be noted that this comparison is prepared for critical buckling load of a simply supported nanobeam for which the material properties $E=30\times10^6$ psi, $\nu=0.3$ are used. Fig. 2 shows

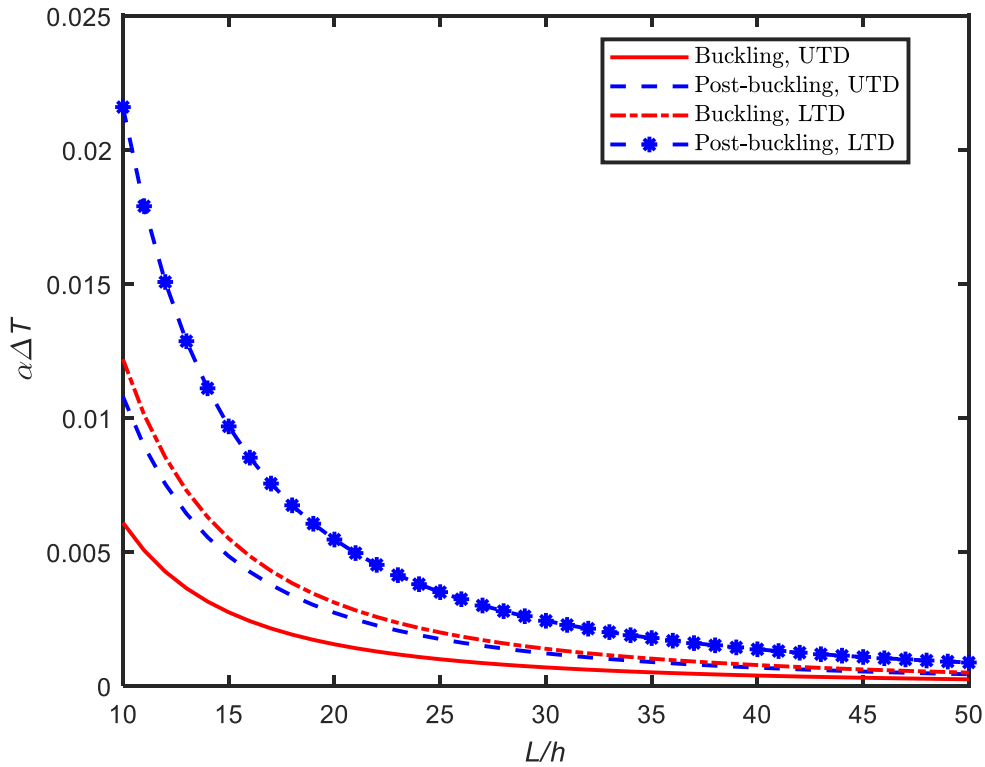

Fig. 4. Non-dimensional buckling ($\widetilde{W}/h = 0$) and post-buckling ($\widetilde{W}/h = 0.5$) temperatures vs. slenderness ratio for the DFM case ($e_0a = h, l = h, W^* = 0$).

Table 2
Non-dimensional critical buckling loads ($\overline{N}_{cr} = N \times (L^2/EI)$) of simply-supported nanobeams.

L/h	μ	Present		Reddy (2007)	
		EBT[a]	TBT[b]	EBT	TBT
100	0	9.8696	9.8671	9.8696	9.8671
	0.5	9.4055	9.4031	9.4055	9.4031
	1	8.9830	8.9807	8.9830	8.9807
	1.5	8.5969	8.5947	8.5969	8.5947
	2	8.2426	8.2405	8.2426	8.2405
20	0	9.8696	9.8067	9.8696	9.8067
	0.5	9.4055	9.3455	9.4055	9.3455
	1	8.9830	8.9258	8.9830	8.9258
	1.5	8.5969	8.5421	8.5969	8.5421
	2	8.2426	8.1900	8.2426	8.1900
10	0	9.8696	9.6227	9.8696	9.6227
	0.5	9.4055	9.1701	9.4055	9.1701
	1	8.9830	8.7583	8.9830	8.7583
	1.5	8.5969	8.3818	8.5969	8.3818
	2	8.2426	8.0364	8.2426	8.0364

[a]Euler–Bernoulli beam theory.
[b]Timoshenko beam theory.

a comparison between the present study and Mirjavadi et al. (2017) for critical temperature change of simply supported axially functionally graded (AFG) nanobeam. All comparisons show very good agreements. It is also worth noting that Reddy (2007) used an analytical method and Mirjavadi et al. (2017) used the generalized differential quadrature method to obtain their results.

5. Numerical results and discussion

After validation of the obtained results from the present study with the existing data in the open literature, the effects of different parameters such as scaling parameters, plate slenderness ratio (length to thickness ratio), mid-plane initial rise, different temperature distributions, and magnetic potential will be explored in detail.

Fig. 3, ($L/h = 10, l/h = 1, w^* = 0$), illustrates the effect of magnetic potential on the thermal buckling and post-buckling behavior of piezomagnetic (PM) nano-plate strips considering the converse flexomagnetic effect. Also, the effect of nonlocality is studied. It is shown that the local model overpredicts the buckling and post-buckling temperatures, and one can see that by increasing the nonlocal parameter, the buckling and post-buckling temperatures decrease, which means the nonlocality causes the stiffness-softening. Increasing the magnetic potential increases the buckling and post-buckling temperatures. Also, the buckling and post-buckling temperatures in the uniform thermal environment are smaller than in the linear one.

Figs. 4 and 5 demonstrate the effect of temperature distributions on the buckling and post-buckling temperatures with changing of the slenderness ratio when $e_0a = l = h, W^* = 0, \Psi_1 = 1$ mA for DFM and CFM cases, respectively. The buckling ($\widetilde{W}/h = 0$) and post-buckling ($\widetilde{W}/h = 0.5$) temperatures of uniform temperature distribution (UTD, $n = 0$) are lower than those of the linear temperature distribution (LTD, $n = 1$). This is obtained due to the fact that in case of UTD, temperature variation through thickness is identical, while temperature varies along with thickness in LTD, therefore, as thickness increases, the increase in buckling and post-buckling temperature loads in LTD is higher than that in UTD. The slenderness ratio plays a crucial role in the designing of sensors and actuators. From these figures, it can be deduced that the greater the slenderness ratio reduces the thermal stability of the nano-sensors and nano-actuators. Also, the effect of temperature distribution is more sensible at lower slenderness ratios for both buckling and post-buckling temperatures. In another word, the effect of temperature distribution vanishes at larger slenderness ratios. Thus, it can be concluded that the effect of temperature distribution is negligible for thinner PFM nano-plate strips.

Fig. 6(a) shows non-dimensional temperature loads for buckling and post-buckling in different non-dimensional nonlocal parameters and dimensionless amplitudes when $l = h, L/h = 40, W^* = 0$, LTD. It is seen that increment of dimensionless amplitude increases the buckling

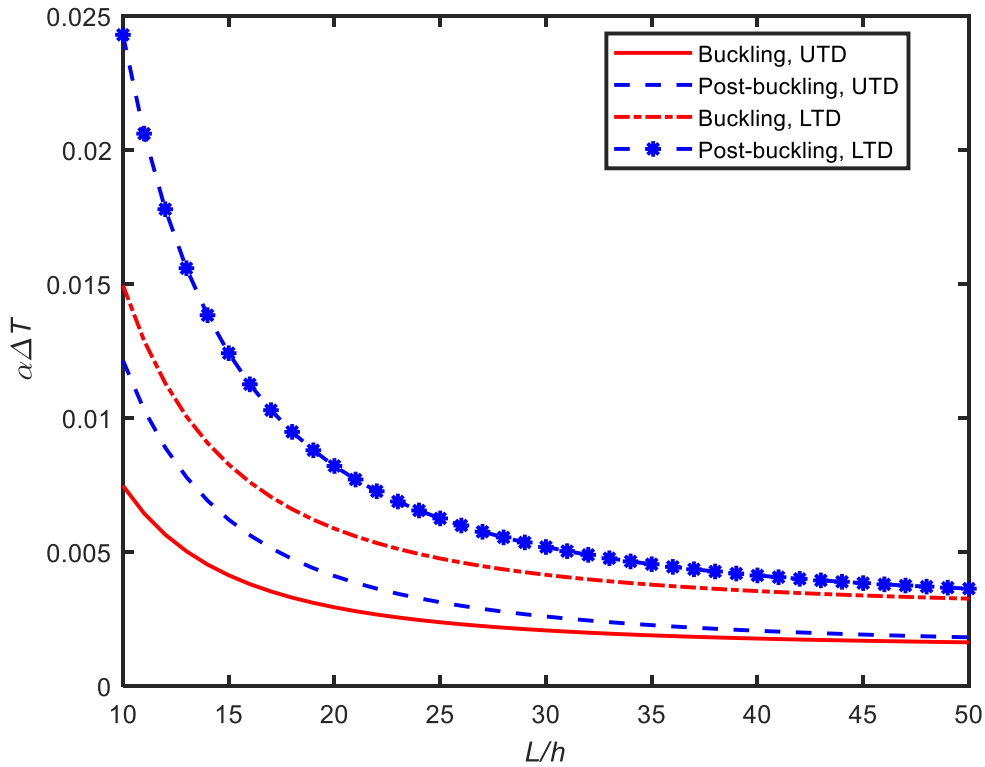

Fig. 5. Non-dimensional buckling ($\widetilde{W}/h = 0$) and post-buckling ($\widetilde{W}/h = 0.5$) temperatures vs. slenderness ratio for the CFM case ($e_0a = h, l = h, W^* = 0, \Psi_1 = 1$ mA).

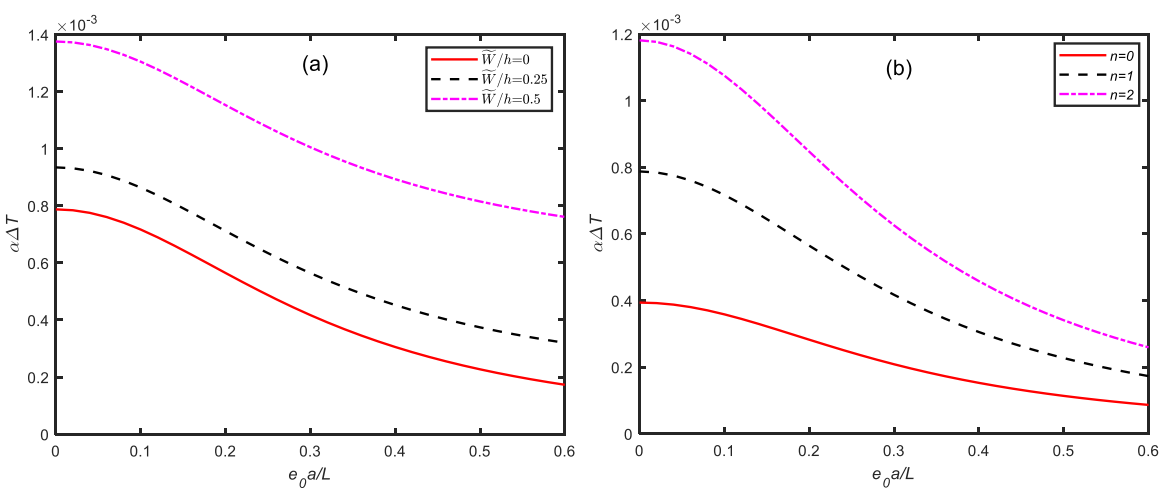

Fig. 6. Non-dimensional buckling and post-buckling temperatures vs. non-dimensional nonlocal parameter ($l = h, L/h = 40, W^* = 0$). (a) Different dimensionless amplitude (LTD), (b) different temperature distributions.

and post-buckling temperatures. In addition, the greater the nonlocal parameter reduces the thermal stability of the PFM nano-sensors and nano-actuators. Fig. 6(b) shows non-dimensional critical temperature in different non-dimensional nonlocal parameters and power indices of temperature variation function (n) when $l = h, L/h = 40, W^* = 0, \widetilde{W} = 0$. It is shown that the thermal stability reduces as the non-dimensional nonlocal parameter increases. Also, the effect of temperature distribution is more sensible at lower nonlocal parameters for critical temperatures. The critical temperature of uniform temperature distribution is the lowest and the nonlinear temperature distribution ($n = 2$) is the highest curve.

The effect of geometrical imperfection in different dimensionless amplitudes on thermal post-buckling loads of PFM nano-actuators (CFM effect) is plotted in Fig. 7 when $e_0a = l = h, \Psi_1 = 1$ mA, $L/h = 50$. As shown, in case of perfect configuration, the PFM nano-plate strip is first critically buckled. Then, the increment of dimensionless amplitude increases thermal stability. In the case of imperfect configuration, the buckling temperature is zero at the starting point and there is no buckling strength before the initial state of the PFM nano-plate strip. After that, the greater dimensionless amplitudes increase the thermal stability. Also, the effect of geometrical imperfection is more considerable at lower dimensionless amplitudes and vanishes at larger amplitudes. The post-buckling temperature loads of imperfect configurations are lower than the perfect configuration.

To study temperature distribution on critical buckling temperature of PFM nano-sensors (DFM effect), this parameter is illustrated for different values of strain gradient parameter in Fig. 8 ($e_0a = h, L/h = 10, W^* = 0, \widetilde{W} = 0$). It is shown that critical buckling

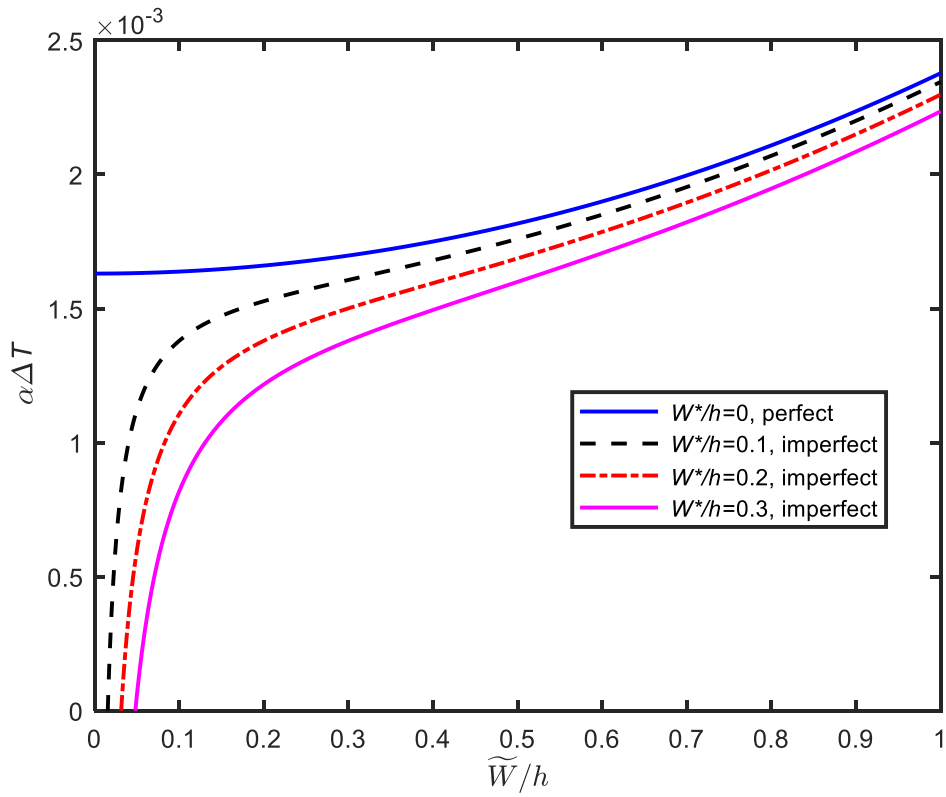

Fig. 7. Non-dimensional thermal post-buckling loads of PFM nano-actuators (CFM effect) vs. dimensionless amplitude in different geometrical imperfections.

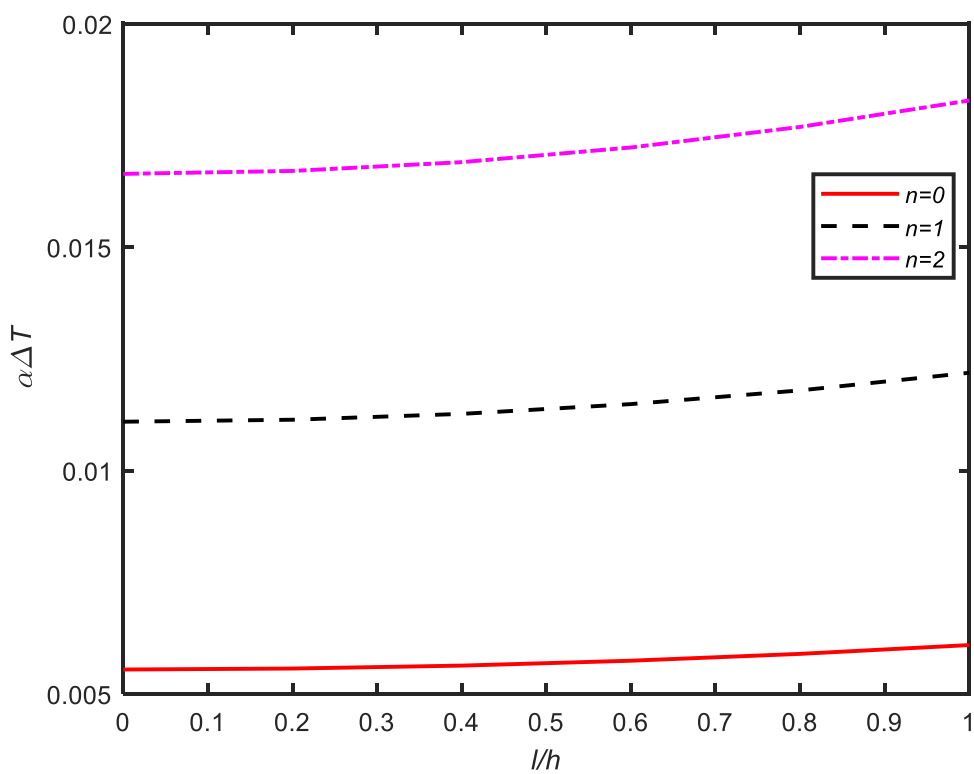

Fig. 8. Non-dimensional critical buckling temperature of PFM nano-sensors (DFM effect) vs. dimensionless strain gradient parameter in different temperature distributions.

temperature increases as n is increased. Also, higher values of the strain gradient parameter increase the thermal stability of the PFM nano-sensors.

The effect of shear deformation on thermal buckling load is plotted in Fig. 9. As expected, the critical temperature of thinner PFM nano-plate strips is identical between the classical and first-order shear

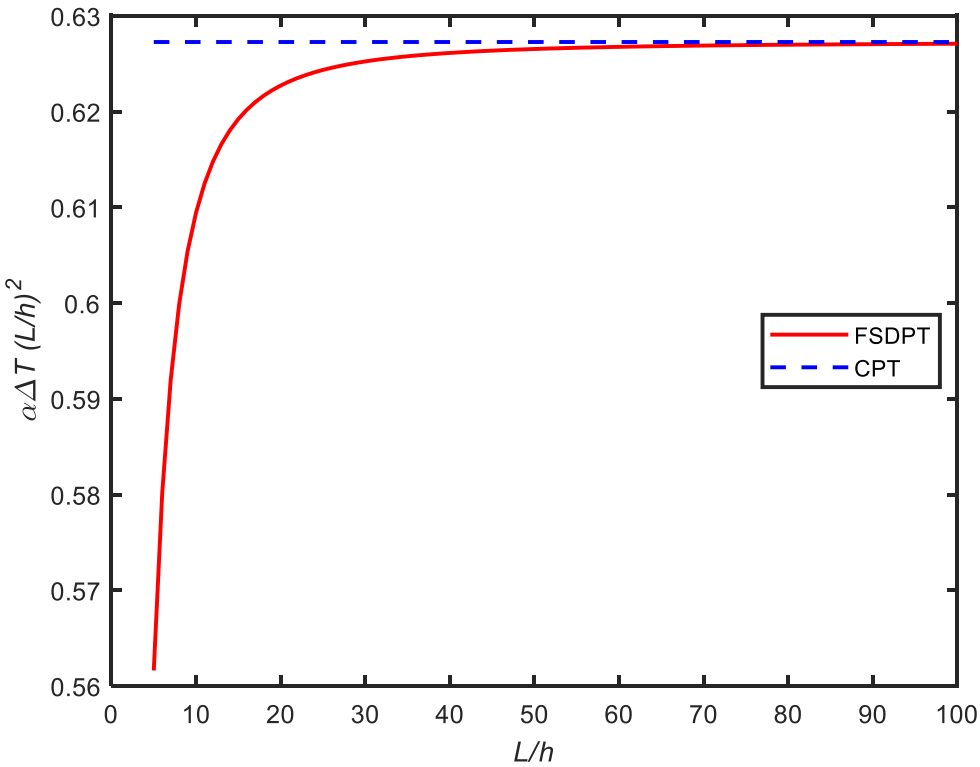

Fig. 9. Effect of shear deformation on dimensionless thermal buckling load of PFM nano-plate strips.

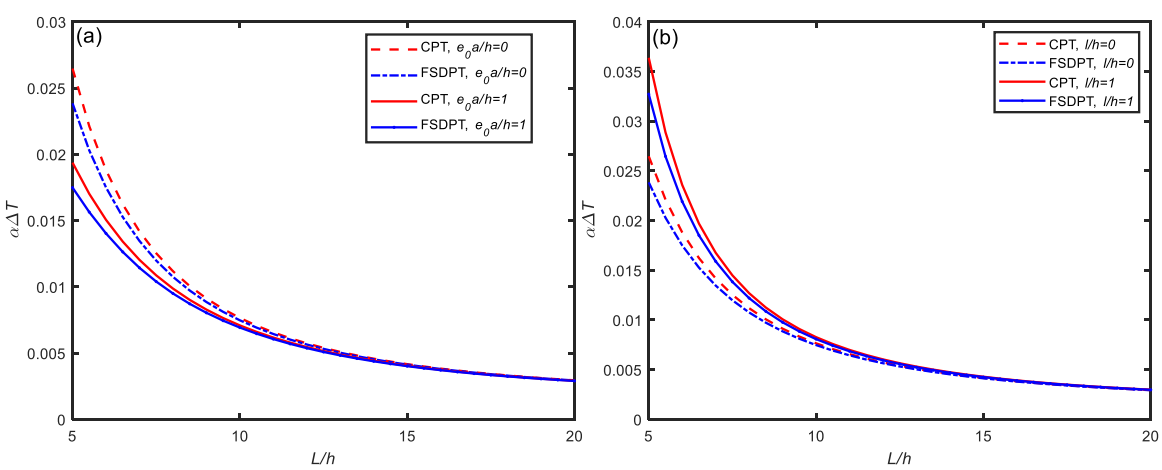

Fig. 10. The critical temperature of the PFM nano-actuators with respect to the slenderness ratio. (a) Different nonlocal parameters, (b) different strain gradient parameters.

deformation plate theories. The difference between the two theories becomes more by increasing the thickness.

Fig. 10 represents the critical temperature of the PFM nano-actuators with respect to the slenderness ratio in different nonlocal and strain gradient parameters. The results are obtained based on the CPT and FSDPT when $\Psi_1 = 1$ mA, $W^* = 0, \widetilde{W} = 0$, and UTD. It is observed that the length scale parameters affect the critical temperature, especially for short nano-plate strips. Increasing the nonlocal parameter decreases the thermal stability while the strain gradient parameter has the opposite effect. In addition, a comparison of the results obtained by the CPT and FSDPT shows that buckling temperatures predicted by the CPT are higher than ones obtained based on the FSDPT for short nano-actuators. Note that the above results converge as the slenderness ratio is increased.

6. Conclusions

Thermal buckling and post-buckling analysis of geometrically imperfect piezomagnetic nano-plate strips considering direct and converse flexomagnetic effects were investigated based on the nonlocal strain gradient theory. Considering the first-order shear deformation plate theory, the governing differential equations, and related boundary conditions were derived using the principle of minimum total potential energy. Afterward, the Navier method was used to obtain the closed-form solution of the problem. Finally, some numerical results were presented and the effect of several parameters on the thermal stability of nano-sensors and nano-actuators was investigated. By controlling these parameters, it is possible to control the performance of the PFM nano-structure and at the same time prevent its buckling. The authors hope that the obtained results may serve as benchmarks for future

analyses of PFM nano-structures, and may be used by scientists in designing and preventing thermal instability in such nano-structures. Numerical results showed that:

- The magnetic potential has a significant effect on the thermal stability.
- Nonlocality and the strain gradient cause the stiffness-softening and the stiffness-hardening, respectively.
- The highest thermal stability is related to quadratic temperature distribution and the lowest is related to the uniform temperature distribution.
- The effect of the mid-plane initial rise is insignificant in larger dimensionless amplitudes.
- The results obtained by the CPT and FSDPT converge as the nano-plate strip becomes thinner. This implicitly confirms the correctness of the relationships obtained.
- The slenderness ratio plays a crucial role in the designing of PFM nano-structures. The greater the slenderness ratio reduces the thermal stability.

CRediT authorship contribution statement

Hamed Momeni-Khabisi: Methodology, Formal analysis, Validation, Writing – original draft, Software. **Masoud Tahani:** Conceptualization, Supervision, Reviewing and editing, Project administration.

Declaration of competing interest

The authors declare that they have no known competing financial interests or personal relationships that could have appeared to influence the work reported in this paper.

Data availability

No data was used for the research described in the article.

Funding

This research did not receive any specific grant from funding agencies in the public, commercial, or not-for-profit sectors.

References

Angelou, A., Norman, C., Miran, N., Albers, S., Moradi-Dastjerdi, R., Behdinan, K., 2021. An eco-friendly, biocompatible and reliable piezoelectric nanocomposite actuator for the new generation of microelectronic devices. Eur. Phys. J. Plus 136 (6), 678. http://dx.doi.org/10.1140/epjp/s13360-021-01653-z.

Bahl, S., Nagar, H., Singh, I., Sehgal, S., 2020. Smart materials types, properties and applications: A review. Mater. Today: Proc. 28, 1302–1306. http://dx.doi.org/10.1016/j.matpr.2020.04.505, URL: https://www.sciencedirect.com/science/article/pii/S2214785320331278, International Conference on Aspects of Materials Science and Engineering.

Barati, M.R., Zenkour, A.M., 2019. Thermal post-buckling analysis of closed circuit flexoelectric nanobeams with surface effects and geometrical imperfection. Mech. Adv. Mater. Struct. 26 (17), 1482–1490. http://dx.doi.org/10.1080/15376494.2018.1432821, arXiv:https://doi.org/10.1080/15376494.2018.1432821.

Basutkar, R., Sidhardh, S., Ray, M., 2019. Static analysis of flexoelectric nanobeams incorporating surface effects using element free Galerkin method. Eur. J. Mech. A Solids 76, 13–24. http://dx.doi.org/10.1016/j.euromechsol.2019.02.013, URL: https://www.sciencedirect.com/science/article/pii/S0997753818305011.

Behdinan, K., Moradi-Dastjerdi, R., 2022. Thermal buckling resistance of a lightweight lead-free piezoelectric nanocomposite sandwich plate. Adv. Nano Res. 12, 593–603. http://dx.doi.org/10.12989/anr.2022.12.6.593, URL: https://koreascience.kr/article/JAKO202218253921110.page.

Cai, R., Antohe, V.-A., Nysten, B., Piraux, L., Jonas, A.M., 2020. Thermally induced flexo-type effects in nanopatterned multiferroic layers. Adv. Funct. Mater. 30 (14), 1910371. http://dx.doi.org/10.1002/adfm.201910371, arXiv:https://onlinelibrary.wiley.com/doi/pdf/10.1002/adfm.201910371 URL: https://onlinelibrary.wiley.com/doi/abs/10.1002/adfm.201910371.

Ebnali Samani, M.S., Tadi Beni, Y., 2018. Size dependent thermo-mechanical buckling of the flexoelectric nanobeam. Mater. Res. Express (Online) 5 (8), 18, URL: http://inis.iaea.org/search/search.aspx?orig_q=RN:51080598, Nanoscience and nanotechnology.

Eliseev, E.A., Morozovska, A.N., Glinchuk, M.D., Blinc, R., 2009. Spontaneous flexoelectric/flexomagnetic effect in nanoferroics. Phys. Rev. B 79, 165433. http://dx.doi.org/10.1103/PhysRevB.79.165433, URL: https://link.aps.org/doi/10.1103/PhysRevB.79.165433.

Eliseev, E.A., Morozovska, A.N., Khist, V.V., Polinger, V., 2019. Chapter six - Effective flexoelectric and flexomagnetic response of ferroics. In: Stamps, R.L., Schultheiß, H. (Eds.), Recent Advances in Topological Ferroics and their Dynamics. In: Solid State Physics, vol. 70, Academic Press, pp. 237–289. http://dx.doi.org/10.1016/bs.ssp.2019.09.002, URL: https://www.sciencedirect.com/science/article/pii/S0081194719300025.

Hu, C., Behdinan, K., Moradi-Dastjerdi, R., 2022. PVDF energy harvester for prolonging the battery life of cardiac pacemakers. Actuators 11 (7), http://dx.doi.org/10.3390/act11070187, URL: https://www.mdpi.com/2076-0825/11/7/187.

Karimiasl, M., Kargarfard, K., Ebrahimi, F., 2019. Buckling of magneto-electro-hygro-thermal piezoelectric nanoplates system embedded in a visco-pasternak medium based on nonlocal theory. Microsyst. Technol. 25 (3), 1031–1042. http://dx.doi.org/10.1007/s00542-018-4082-0.

Malikan, M., Eremeyev, V.A., 2022a. The effect of shear deformations' rotary inertia on the vibrating response of multi-physic composite beam-like actuators. Compos. Struct. 297, 115951. http://dx.doi.org/10.1016/j.compstruct.2022.115951, URL: https://www.sciencedirect.com/science/article/pii/S0263822322007085.

Malikan, M., Eremeyev, V.A., 2022b. On a flexomagnetic behavior of composite structures. Internat. J. Engrg. Sci. 175, 103671. http://dx.doi.org/10.1016/j.ijengsci.2022.103671, URL: https://www.sciencedirect.com/science/article/pii/S0020722522000441.

Malikan, M., Uglov, N.S., Eremeyev, V.A., 2020. On instabilities and post-buckling of piezomagnetic and flexomagnetic nanostructures. Internat. J. Engrg. Sci. 157, 103395. http://dx.doi.org/10.1016/j.ijengsci.2020.103395, URL: https://www.sciencedirect.com/science/article/pii/S0020722520301828.

Malikan, M., Wiczenbach, T., Eremeyev, V.A., 2021. On thermal stability of piezo-flexomagnetic microbeams considering different temperature distributions. Contin. Mech. Thermodyn. 33 (4), 1281–1297. http://dx.doi.org/10.1007/s00161-021-00971-y.

Malikan, M., Wiczenbach, T., Eremeyev, V.A., 2021b. Thermal buckling of functionally graded piezomagnetic micro- and nanobeams presenting the flexomagnetic effect. Contin. Mech. Thermodyn. http://dx.doi.org/10.1007/s00161-021-01038-8.

Maurya, K.K., Rawat, A., Jha, G., 2020. Smart materials and electro-mechanical impedance technique: A review. Mater. Today: Proc. 33, 4993–5000. http://dx.doi.org/10.1016/j.matpr.2020.02.831, URL: https://www.sciencedirect.com/science/article/pii/S2214785320316217, 2nd International Conference on Processing and Characterization of Materials.

Meschino, M., Wang, L., Xu, H., Moradi-Dastjerdi, R., Behdinan, K., 2021. Low-frequency nanocomposite piezoelectric energy harvester with embedded zinc oxide nanowires. Polym. Compos. 42 (9), 4573–4585. http://dx.doi.org/10.1002/pc.26169, arXiv:https://onlinelibrary.wiley.com/doi/pdf/10.1002/pc.26169 URL: https://onlinelibrary.wiley.com/doi/abs/10.1002/pc.26169.

Mir, M., Tahani, M., 2020. Graphene-based mass sensors: Chaotic dynamics analysis using the nonlocal strain gradient model. Appl. Math. Model. 81, 799–817. http://dx.doi.org/10.1016/j.apm.2020.01.022, URL: https://www.sciencedirect.com/science/article/pii/S0307904X20300226.

Mirjavadi, S.S., Rabby, S., Shafiei, N., Afshari, B.M., Kazemi, M., 2017. On size-dependent free vibration and thermal buckling of axially functionally graded nanobeams in thermal environment. Appl. Phys. A 123 (5), 315. http://dx.doi.org/10.1007/s00339-017-0918-1.

Momeni-Khabisi, H., Tahani, M., 2022. A size-dependent study on buckling and post-buckling behavior of imperfect piezo-flexomagnetic nano-plate strips. Adv. Nano Res. 12 (4), 427–440. http://dx.doi.org/10.12989/ANR.2022.12.4.427.

Moradi, R., Behdinan, K., 2020. Thermo-electro-mechanical behavior of an advanced smart lightweight sandwich plate. Aerosp. Sci. Technol. 106, 106142. http://dx.doi.org/10.1016/j.ast.2020.106142, URL: https://www.sciencedirect.com/science/article/pii/S1270963820308245.

Moradi, R., Behdinan, K., 2021. Temperature effect on free vibration response of a smart multifunctional sandwich plate. J. Sandw. Struct. Mater. 23 (6), 2399–2421. http://dx.doi.org/10.1177/1099636220908707, arXiv:https://doi.org/10.1177/1099636220908707.

Moradi-Dastjerdi, R., Behdinan, K., 2021. Dynamic performance of piezoelectric energy harvesters with a multifunctional nanocomposite substrate. Appl. Energy 293, 116947. http://dx.doi.org/10.1016/j.apenergy.2021.116947, URL: https://www.sciencedirect.com/science/article/pii/S0306261921004244.

Moradi-Dastjerdi, R., Meguid, S., Rashahmadi, S., 2019. Electro-dynamic analysis of smart nanoclay-reinforced plates with integrated piezoelectric layers. Appl. Math. Model. 75, 267–278. http://dx.doi.org/10.1016/j.apm.2019.05.033, URL: https://www.sciencedirect.com/science/article/pii/S0307904X19303300.

Nicolenco, A., de h ra, M., Yun, C., MacManus-Driscoll, J., Sort, J., 2021. Strain-gradient effects in nanoscale-engineered magnetoelectric materials. APL Mater. 9 (2), 020903. http://dx.doi.org/10.1063/5.0037421, arXiv:https://doi.org/10.1063/5.0037421.

Rasilo, P., Aydin, U., Martin, F., Belahcen, A., Kouhia, R., Daniel, L., 2019. Equivalent strain and stress models for the effect of mechanical loading on the permeability of ferromagnetic materials. IEEE Trans. Magn. 55 (6), 1–4. http://dx.doi.org/10.1109/TMAG.2018.2890407.

Reddy, J.N., 2006. Theory and Analysis of Elastic Plates and Shells, second ed. CRC Press, URL: https://doi.org/10.1201/9780849384165.

Reddy, J.N., 2007. Nonlocal theories for bending, buckling and vibration of beams. Internat. J. Engrg. Sci. 45 (2), 288–307. http://dx.doi.org/10.1016/j.ijengsci.2007.04.004, URL: https://www.sciencedirect.com/science/article/pii/S0020722507000377.

Shi, Y., Li, N., Ye, J., Ma, J., 2021. Enhanced magnetoelectric response in nanostructures due to flexoelectric and flexomagnetic effects. J. Magn. Magn. Mater. 521, 167523. http://dx.doi.org/10.1016/j.jmmm.2020.167523, URL: https://www.sciencedirect.com/science/article/pii/S0304885320324902.

Sidhardh, S., Ray, M.C., 2018. Flexomagnetic response of nanostructures. J. Appl. Phys. 124 (24), 244101. http://dx.doi.org/10.1063/1.5060672.

Tocci Monaco, G., Fantuzzi, N., Fabbrocino, F., Luciano, R., 2021. Hygrothermal vibrations and buckling of laminated nanoplates via nonlocal strain gradient theory. Compos. Struct. 262, 113337. http://dx.doi.org/10.1016/j.compstruct.2020.113337, URL: https://www.sciencedirect.com/science/article/pii/S0263822320332633.

Wang, S., Kang, W., Yang, W., Zhang, Z., Li, Q., Liu, M., Wang, X., 2022. Hygrothermal effects on buckling behaviors of porous bi-directional functionally graded micro-/nanobeams using two-phase local/nonlocal strain gradient theory. Eur. J. Mech. A Solids 94, 104554. http://dx.doi.org/10.1016/j.euromechsol.2022.104554, URL: https://www.sciencedirect.com/science/article/pii/S0997753822000432.

Wang, B., Li, X.-F., 2021. Flexoelectric effects on the natural frequencies for free vibration of piezoelectric nanoplates. J. Appl. Phys. 129 (3), 034102. http://dx.doi.org/10.1063/5.0032343.

Wei, Y., Xu, Q., 2015. An overview of micro-force sensing techniques. Sensors Actuators A 234, 359–374. http://dx.doi.org/10.1016/j.sna.2015.09.028, URL: https://www.sciencedirect.com/science/article/pii/S092442471530145X.

Zhang, N., Zheng, S., Chen, D., 2019. Size-dependent static bending of flexomagnetic nanobeams. J. Appl. Phys. 126 (22), 223901. http://dx.doi.org/10.1063/1.5128940.

Zhang, N., Zheng, S., Chen, D., 2022a. Size-dependent static bending, free vibration and buckling analysis of curved flexomagnetic nanobeams. Meccanica 57 (7), 1505–1518. http://dx.doi.org/10.1007/s11012-022-01506-8.

Zhang, N., Zheng, S., Chen, D., 2022b. Size-dependent static bending, free vibration and buckling analysis of simply supported flexomagnetic nanoplates. J. Braz. Soc. Mech. Sci. Eng. 44 (6), 253. http://dx.doi.org/10.1007/s40430-022-03556-1.